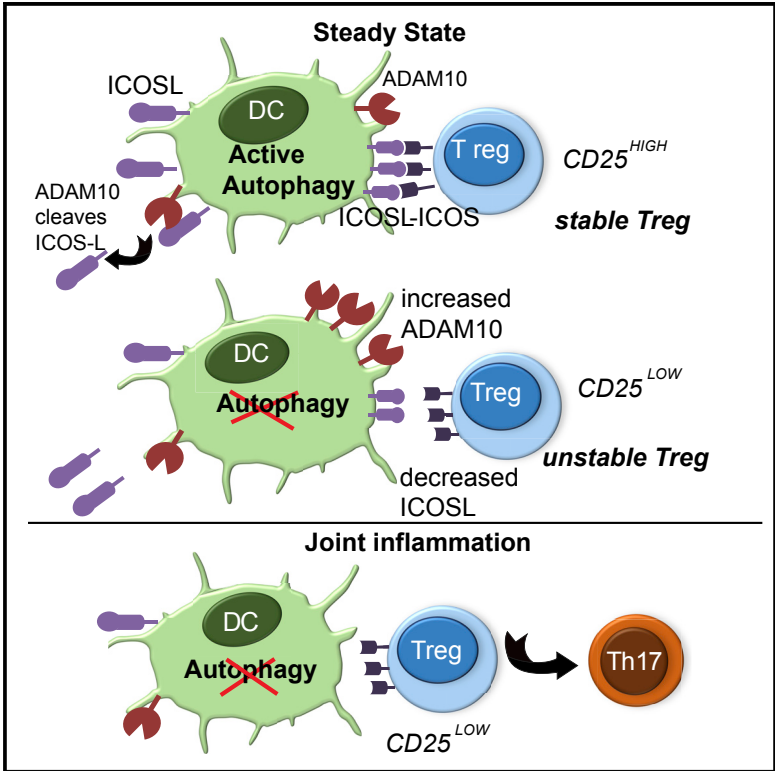


Macroautophagy in Dendritic Cells Controls the Homeostasis and Stability of Regulatory T Cells

Graphical Abstract



Authors

Jennifer Niven, Natacha Madelon, Nicolas Page, ..., Christian A. Seemayer, Stéphanie Hugues, Monique Gannagé

Correspondence

monique.ghannage@chuv.ch

In Brief

Regulatory T cells (Tregs) play a crucial role in controlling autoimmune and inflammatory responses. The homeostasis and stability of Tregs are controlled by dendritic cells. Niven et al. show that autophagy deficiency in dendritic cells can compromise the stability and function of Tregs and precipitate autoimmune and inflammatory disorders.

Highlights

- Tregs from mice with $Atg5^{-/-}$ DCs have reduced suppressive function and stability
- $Atg5^{-/-}$ DCs form less-stable conjugates with Tregs
- ICOS-Ligand expression is decreased in $Atg5^{-/-}$ DCs
- Upon antigen-induced arthritis, Tregs convert to Th17 in $Atg5^{-/-}$ DC mice

Data Resources

GSE98961



Macroautophagy in Dendritic Cells Controls the Homeostasis and Stability of Regulatory T Cells

Jennifer Niven,^{1,2} Natacha Madelon,^{1,2,4} Nicolas Page,¹ Assunta Caruso,^{1,2} Guillaume Harlé,¹ Sylvain Lemeille,¹ Christian A. Seemayer,³ Stéphanie Hugues,¹ and Monique Gannage^{1,2,4,5,*}

¹Department of Pathology and Immunology, School of Medicine, University of Geneva, 1211, Geneva 4, Switzerland

²Division of Rheumatology, Department of Internal Medicine, University Hospital, 1211 Geneva 4, Switzerland

³Translational Medicine, Galapagos, 4051 Basel, Switzerland

⁴Present address: Service of Immunology and Allergy, Lausanne University Hospital, University of Lausanne, 1011 Lausanne, Switzerland

⁵Lead Contact

*Correspondence: monique.ghannage@chuv.ch

<https://doi.org/10.1016/j.celrep.2019.05.110>

SUMMARY

Regulatory T cells (Tregs) play a crucial role in controlling autoimmune and inflammatory responses. Recent studies have demonstrated that dendritic cells (DCs) contribute to the homeostasis of peripheral Tregs. Autophagy, a critical pathway for cellular homeostasis, is active in DCs and is upregulated in different inflammatory conditions. We have shown that Tregs are expanded and have phenotypic alterations and impaired suppressive functions in mice with autophagy-deficient DCs. RNA profiling of Tregs revealed that autophagy in DCs is required to stabilize Treg expression signatures. This phenotype is linked to the downregulation of ICOS-Ligand expression in autophagy-deficient DCs, a consequence of the accumulation of ADAM10, the metalloproteinase responsible for its cleavage. Upon inflammation, in antigen-induced arthritis, mice with autophagy-deficient DCs exhibit increased synovial inflammation and cartilage and bone erosion correlating with Treg-to-Th17 conversion. Our data reveal a mechanism that couples autophagy deficiency in DCs to the function, homeostasis, and stability of Tregs.

INTRODUCTION

Regulatory T cells (Tregs) play a crucial role in controlling autoimmune and inflammatory responses (Josefowicz et al., 2012; Kim et al., 2007). The molecular signature of Tregs is characterized by the expression of the forkhead box transcription factor (Foxp3), which is essential to their maintenance and function (Fontenot et al., 2003). A stable expression of Foxp3 in Tregs is therefore crucial for ensuring Treg function, limiting autoimmunity, and maintaining self-tolerance. Indeed, several reports have challenged the stability of Tregs and demonstrated their conversion toward Th1/Th17 and, more recently, toward Th2 cells. In this context, Tregs downregulate the expression of Foxp3. These ob-

servations were facilitated by the use of fate-mapping Tregs, which allowed us to unambiguously demonstrate the plasticity of these cells *in vivo*. Initial studies have shown that Tregs could become unstable in a lymphopenic environment and lose the expression of Foxp3 (Duarte et al., 2009; Komatsu et al., 2009). These findings were controversial, as they could solely account for a deprivation in interleukin-2 (IL-2) that is necessary to sustain Tregs' stability. Later studies, however, have demonstrated the Th1/Th17 conversion of Tregs using fate-reporter cells in mouse models of three autoimmune diseases: experimental autoimmune encephalomyelitis (Bailey-Bucktrout et al., 2013), type 1 diabetes (Zhou et al., 2009), and collagen-induced arthritis (Komatsu et al., 2014). In parallel, upon exposure to inflammatory stimuli *in vitro*, Tregs can lose Foxp3 expression and differentiate into effector Th17, Th1, or Th2 cells (Hoffmann et al., 2009; Xu et al., 2007). These findings were also recapitulated in human Tregs, which lose Foxp3 expression upon T cell receptor (TCR) stimulation in the presence of pro-inflammatory cytokines (Koenen et al., 2008). In addition, unstable Tregs were detected in several autoimmune diseases, such as type 1 diabetes (Long et al., 2010), systemic lupus erythematosus (Valencia et al., 2006), and psoriasis (Bovenschen et al., 2011).

Therefore, understanding which factors can control the stability and plasticity of Tregs is crucial in the context of autoimmunity. Several studies have focused on identifying such intrinsic factors. Among them, epigenetically marked *cis*-elements, such as the conserved noncoding sequence 2 (CNS2) of the *Foxp3* gene (Feng et al., 2014), are essential for Treg stability. Other intrinsic important factors such as TCR signaling (Levine et al., 2014), Neuropilin-1 expression (Overacre-Delgoffe et al., 2017), or IL-2 receptor signaling (Chinen et al., 2016) were also demonstrated to be crucial for maintaining Treg identity. While the majority of these studies have focused on identifying intrinsic factors that control Treg function and stability, limited work has focused on identifying such extrinsic factors. In that aspect, different groups have reported a direct role of antigen-presenting cells (APCs) on the homeostasis of natural or antigen-induced Tregs. Indeed, Tregs were shown to interact with both conventional and plasmacytoid dendritic cells (DCs) (Darrasse-Jèze et al., 2009; Ito et al., 2007) in the context of



autoimmunity or tumors. In both instances, these interactions were beneficial for the function and maintenance of Tregs.

We were interested in the role of DCs in controlling Treg compartments. We focused more precisely on the potential role of the macroautophagy pathway (hereafter referred as autophagy) in DCs on Tregs' phenotypes and functions. The autophagy pathway has been critically involved in APCs to control aspects of both innate and adaptive immune responses in various contexts of inflammation or pathogen infections (Deretic et al., 2013). Indeed, targeted deletion of autophagy in DCs has been shown to modulate CD4 and CD8 T cell responses in different infectious models. However, few studies have described a contribution of the pathway in APCs to peripheral tolerance.

Here, we show that autophagy in DCs is required for Treg homeostasis and function both in steady state and upon inflammation. This phenotype is linked to a decreased expression of ICOS-Ligand (ICOS-L) in autophagy-deficient DCs, a co-stimulatory molecule that is crucial for Tregs' maintenance and effector function (Burmeister et al., 2008; Redpath et al., 2013). As a consequence, in the absence of autophagy in DCs, Tregs are dysfunctional and unstable, leading to disease exacerbation in a mouse model of rheumatoid arthritis (RA). Our study identifies a mechanism by which autophagy in DCs contributes to the maintenance of peripheral T cell tolerance.

RESULTS AND DISCUSSION

Tregs from *Atg5*^{-/-} DC Mice Are Expanded and Show an Activated and Effector Phenotype

We analyzed, in the steady state, the Treg compartment in mice with autophagy-deficient DCs (*Atg5*^{-/-} DC mice). We found that compared to their littermate controls, *Atg5*^{-/-} DC mice had increased frequencies and absolute numbers of total Tregs in their secondary lymphoid organs (SLOs) (Figures 1A, S1A, and S1B). This observation correlates with increased peripheral proliferation of Tregs in *Atg5*^{-/-} DC mice (Figures 1B and 1C). Interestingly, the frequency of Neuropilin-1⁺ Tregs was also increased in the periphery (Figure S1C), suggesting that this phenotype was related to natural Tregs' proliferation. We then analyzed if a particular subset of Tregs was expanded in *Atg5*^{-/-} DC mice. We found an increase in the percentage and absolute numbers of CD25^{Low} and CD25^{Neg} Treg subsets in SLO, while the absolute counts of CD25^{High} Tregs remained unchanged (Figures 1D, 1E, and S1D).

All these changes did not affect thymic Tregs since the frequency, proliferation, and CD25 subsets of Tregs remained unchanged in the thymus of *Atg5*^{-/-} DC mice (Figures S1E and S1F).

We next analyzed the phenotype of Tregs in *Atg5*^{-/-} DC mice and their littermate controls. We found that *Atg5*^{-/-} DC mice had a significantly increased frequency of effector Tregs in the steady state (CD44^{High} CD62^{Low} Tregs) (Figures 1F and 1G), a subset of Tregs that is enriched in CD25^{Low} and CD25^{Neg} Tregs (Figure S1G) as well as in activated Tregs (Figure S1H) (Fontenot et al., 2005). Accordingly, Tregs in *Atg5*^{-/-} DC mice were enriched in ICOS and CD103 effector markers (Figure 1H). In addition, Ly-6C surface expression was significantly lower in Tregs

from *Atg5*^{-/-} DC mice, compared to control mice (Figure 1I), its downregulation being a hallmark of TCR-signaling events (Delpoux et al., 2014). These changes in frequency and phenotype were restricted to Tregs, since the frequencies of memory and naive CD4⁺ Foxp3^{Neg} cells were unchanged in the SLOs of *Atg5*^{-/-} DC mice (Figure S1I). Finally, we could replicate this phenotype in *Atg14*^{-/-} DC mice, which lack *Atg14*, another autophagy-essential gene in their DCs. Indeed, *Atg14*^{-/-} DC mice display a higher frequency of Tregs in their SLOs (Figure S2A) and are enriched in CD25^{Low} and CD25^{Neg} subsets (Figure S2B), as well as in their effector Treg subset (Figure S2C). We therefore concluded that mice lacking autophagy in their DCs are enriched in activated and effector Tregs in their SLOs, compared to their littermate controls.

Autophagy in DCs Regulates Treg Function and Stability

To investigate the relevance of these phenotypic changes, we assessed the function of Tregs from *Atg5*^{-/-} DC and *Atg5*^{+/+} DC mice by *in vitro* suppression assay. Surprisingly, we found that Tregs from *Atg5*^{-/-} DC mice, although enriched in effector markers, had a reduced suppressive function (Figure 2A). However, several studies have narrowed down the population of unstable Tregs to CD25^{Low/Neg} subsets (Komatsu et al., 2014; Miyao et al., 2012; Zhou et al., 2009) that are enriched in *Atg5*^{-/-} DC mice. To address the hypothesis of Treg instability, we performed RNA profiling of CD25^{High} and CD25^{Low} Treg subsets from both *Atg5*^{+/+} DC and *Atg5*^{-/-} DC mice. We found differential gene expressions in the CD25^{High} subset and, to a much lower extent, in the CD25^{Low} subset of Tregs (Figures 2B and S2D–S2G). We therefore focused our analysis on the CD25^{High} subset. We first determined whether CD25^{High} Tregs from *Atg5*^{-/-} DC mice share a gene expression profile with unstable CD25^{Low} Tregs generated in *Atg5*^{+/+} DC mice. Gene set enrichment analysis (GSEA) revealed that genes upregulated in CD25^{High} Tregs from *Atg5*^{-/-} DC mice were enriched in the CD25^{Low} signature (Figures 2C and 2D). Since the CNS2 of the Foxp3 gene, a CpG-rich Foxp3 intronic *cis*-element, has been described to be essential for Tregs' stability (Feng et al., 2014; Li et al., 2014) and Foxp3 maintenance, we decided to apply the GSEA of CNS2 knockout (KO) Tregs to our RNA sequencing data. GSEA revealed a significant enrichment in genes from the CNS2 KO Tregs' signature (Figure 2E). Finally, selected GSEAs of conventional T cell (Tconv) signatures were also enriched in our Tregs (Figure 2F), serving as additional evidence that Tregs from *Atg5*^{-/-} DC mice could be unstable and more prone to convert to effector T cells.

We next addressed the molecular mechanism that may account for Tregs' dysfunction and instability in *Atg5*^{-/-} DC mice. We screened for potential genes involved in Tregs' stability through our RNA profiling analysis. We found a significantly higher expression of the genes *Hspa1a* and *Hspa1b* encoding for the heat shock protein 70 (HSP70) in CD25^{High} and CD25^{Low} Tregs isolated from *Atg5*^{-/-} DC mice (Figures 2B and S2E). Since recent publications have shown the involvement of the STUB1-HSP70 complex in promoting FOXP3 ubiquitination and proteasomal degradation (Chen et al., 2013), we investigated the protein expression of HSP70 in Tregs upon TCR activation or exposure to inflammatory stimuli. Confirming the RNA

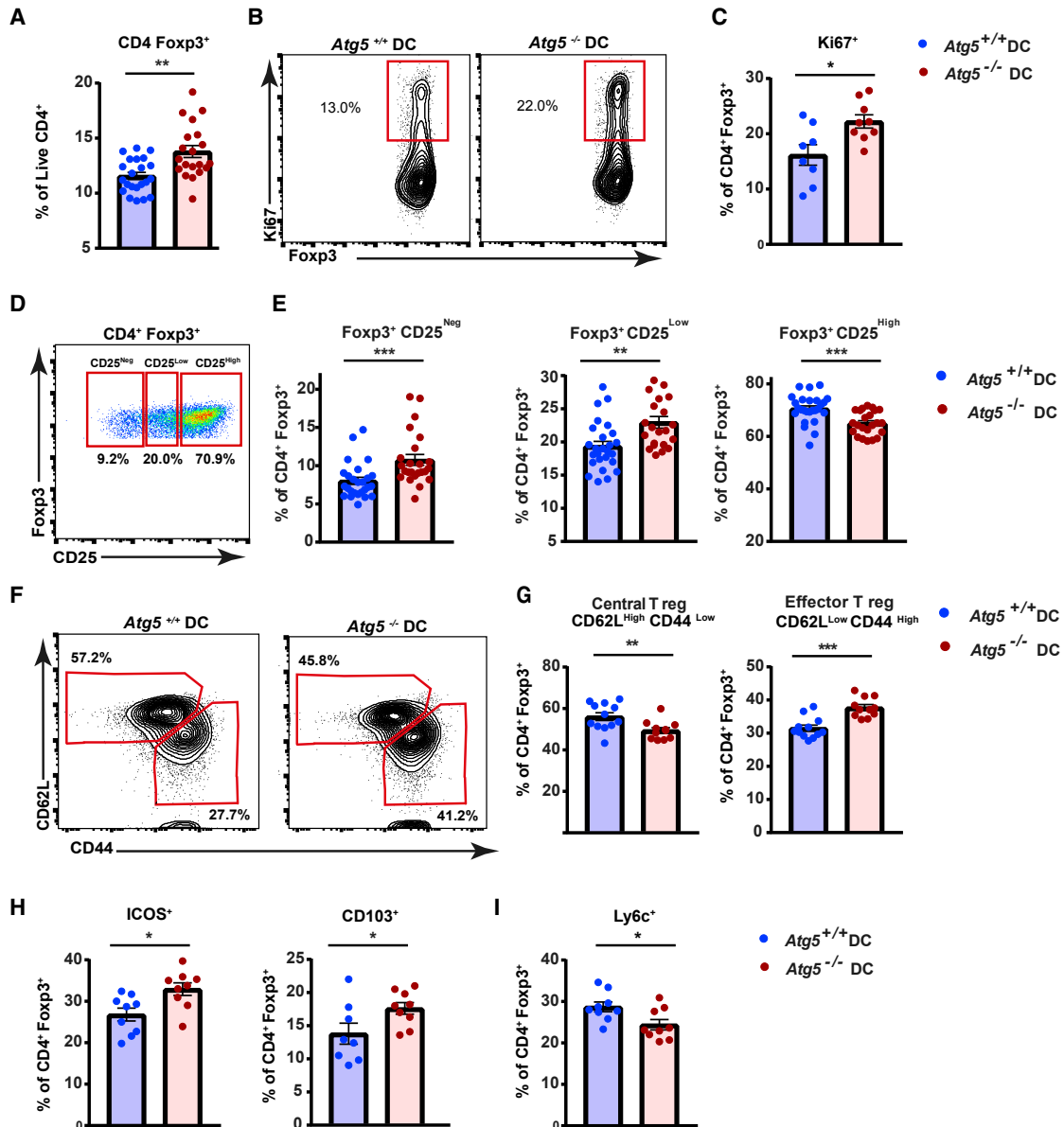


Figure 1. Mice Lacking Autophagy in their DCs Have an Altered Regulatory T Cell Compartment

(A) Flow cytometry analysis of Foxp3⁺ CD4⁺ population in live CD4⁺ splenocytes of *Atg5*^{+/+} DC and *Atg5*^{-/-} DC mice. Bar graph indicates the mean of frequency; each dot represents an individual mouse. Data are a combination of six experiments with 3–7 mice per group.

(B) Representative fluorescence-activated cell sorting (FACS) plots showing the percentage of Ki67⁺ cells within CD4⁺ Foxp3⁺ splenocytes of *Atg5*^{+/+} DC and *Atg5*^{-/-} mice.

(C) Bar graph indicates the mean of frequency of Ki67⁺. Data are a combination of three experiments with 3 mice per group.

(D) Representative FACS plot showing the gating strategy of the three subsets of Foxp3⁺ CD4⁺ cells according to CD25 expression (negative, low, and high).

(E) Bar graphs indicate the mean of frequency of the three subsets of cells in *Atg5*^{+/+} DC and *Atg5*^{-/-} DC mice. Data are a combination of six experiments with 3–7 mice per group.

(F) Representative FACS plots showing the frequency of effector Tregs (CD44^{High} CD62L^{Low}) and central Tregs (CD62L^{High} and CD44^{Low}) in CD4⁺ Foxp3⁺ cells from *Atg5*^{+/+} DC and *Atg5*^{-/-} DC mice.

(G) Bar graphs represent the mean of frequency of the two Treg subsets. Data are from four experiments with 3 mice per group.

(H and I) Flow cytometry analysis of the expression of (H) ICOS⁺, CD103⁺, and (I) Ly6c⁺ in CD4⁺ Foxp3⁺ cells. Bar graphs indicate the mean of frequency of each marker in *Atg5*^{+/+} DC and *Atg5*^{-/-} DC mice. Data are from three individual experiments with 3 mice per group. *p < 0.05; **p < 0.01; ***p < 0.001 (Mann-Whitney test).

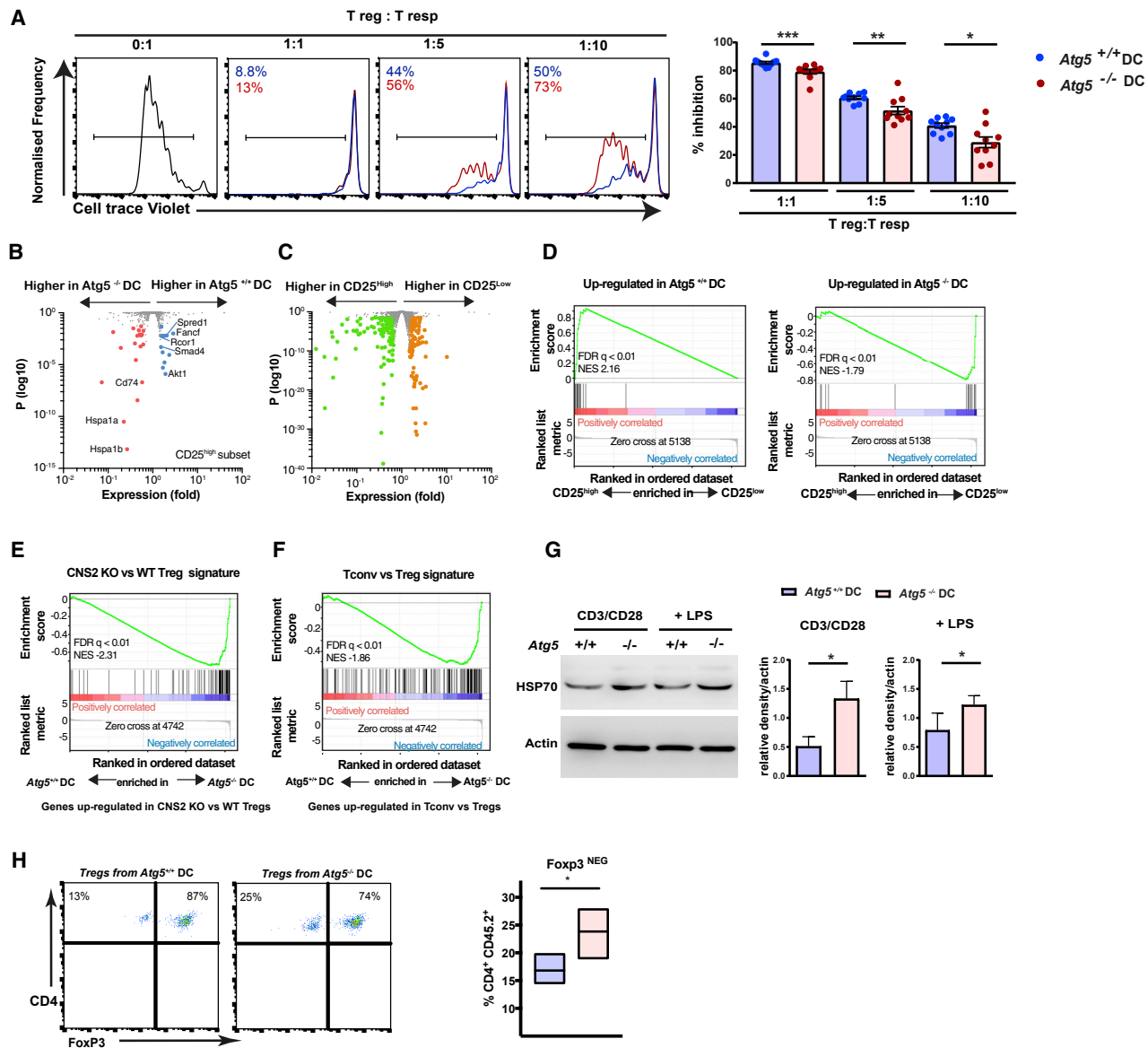


Figure 2. Autophagy in DCs Regulates Treg Function and Stability

(A) Left: representative FACS plots of an *in vitro* suppression assay using Tregs isolated from *Atg5*^{+/+} DC or *Atg5*^{-/-} DC mice and co-cultured with cell trace violet (CTV) labeled CD4⁺ CD45.1⁺ responder T cells (Tresps). Proliferation of Tresps was assessed by the percentage of CTV low population. Right: percentage of inhibition of different ratios (Treg:Tresp) at day 5. The 100% proliferation is set to the 1:0 ratio of Tresp:Treg. Combined data are from two independent experiments with 4–6 replicates per group.

(B) Volcano plot comparing differential gene expression in CD25^{High} Tregs isolated from secondary lymphoid organs of *Atg5*^{+/+} DC and *Atg5*^{-/-} DC mice. Data are combined from three individual replicates with 3–4 mice per replicate.

(C) Volcano plot comparing differential gene expression in CD25^{High} and CD25^{Low} Tregs isolated from secondary lymphoid organs of *Atg5*^{+/+} DC mice. Data are combined from three individual replicates with 3–4 mice per replicate.

(D) Gene set enrichment analysis (GSEA) of *Atg5*-dependent CD25^{High} Treg signature (obtained from RNA-seq data as in B) showing genes induced in CD25^{High} Tregs from *Atg5*^{+/+} DC mice (left) or from *Atg5*^{-/-} DC mice (right). FDR, false discovery rate; NES, normalized enrichment score.

(E and F) GSEA of genes upregulated in CNS2 KO versus WT Tregs (GSE 57272) (E) or Tconv versus Treg (GSE 14415) signatures (F) showing genes induced in CD25^{High} Tregs isolated from *Atg5*^{-/-} DC mice and *Atg5*^{+/+} DC mice.

(G) Western blot analysis of HSP70 expression from CD25^{High} Tregs isolated from *Atg5*^{+/+} and *Atg5*^{-/-} DC mice. Tregs were activated with CD3/CD28 antibodies ± LPS for 24 h. One representative immunoblot is shown. Bar graphs indicate the relative density (mean ± SEM) of HSP70 expression related to β-actin. Data are from three independent experiments. *p < 0.05; ***p < 0.001 (Mann-Whitney test).

(H) Tregs from *Atg5*^{-/-} DC mice or *Atg5*^{+/+} mice were labeled with CTV and adoptively transferred to CD45.1/OT-II host mice. Left: representative FACS plots showing the expression of Foxp3 at day 14 post transfer. Cells were gated on live CD4⁺ CD45.2⁺ CTV^{Low}. Right: bar graphs indicate the mean frequency of Foxp3^{NEG} cells among CD4⁺ CD45.2⁺ cells. Data are a combination of three independent experiments.

sequencing data, western blot analysis revealed a significantly higher expression of HSP70 in Tregs isolated from *Atg5*^{-/-} DC mice upon TCR stimulation (CD3/CD28) or inflammatory stimuli (lipopolysaccharide [LPS]) (Figure 2G), while the level of HSP70 remained very low in the steady state (data not shown). We therefore concluded that Tregs from *Atg5*^{-/-} DC mice have a higher expression of HSP70 upon activation that might result in enhanced FOXP3 degradation in the context of proliferation, TCR activation (Gabryšová et al., 2011), or inflammation. Accordingly, Tregs from *Atg5*^{-/-} DC mice lose significantly more FOXP3 expression after 2 weeks of transfer to CD45.1/OT-II host mice (Figure 2H).

Autophagy Deficiency in DCs Alters the Expression of ICOS-L That Is Crucial for DC-Treg Interactions

We hypothesized that the functional and phenotypic alterations of the Treg compartment in *Atg5*^{-/-} DC was secondary to changes in DC-Treg interactions. Indeed, immature DCs have been shown to form prolonged interactions with Tregs compared to Tconvs, an interaction that results in their increased sensitivity to limiting amounts of antigens (Sarris et al., 2008). In parallel, in the steady state, *in vivo*, Tregs were shown to cluster with migratory DCs in the lymph node (LN) paracortex (Liu et al., 2015). Interestingly, this clustering is dependent on TCR expression on the Tregs. Live cell imaging analysis revealed that *Atg5*^{-/-} DCs form less-stable conjugates with wild-type Tregs compared to *Atg5*^{+/+} DCs (Figure 3A, left). Indeed, the mean duration of contact between Tregs and *Atg5*^{-/-} DCs was significantly reduced compared to *Atg5*^{+/+} DCs, while no difference was observed for the population of conventional CD4⁺ T cells (Figure 3A, right). This phenotype could be related to the regulation by the autophagy pathway of either MHC class II expression or a co-stimulatory molecule involved in DC-Treg contact. Indeed, autophagy has been shown to contribute to the pool of MHC class II peptides by delivering intracellular proteins to the MHC class II compartment (Schmid et al., 2007). In parallel, the regulation of the expression of co-stimulatory molecules by autophagy has already been described in the context of inflammation, upon graft-versus-host disease (Hubbard-Lucey et al., 2014). We did not find a difference in the expression level of MHC class II molecules in *Atg5*^{-/-} DCs; therefore, we analyzed in the steady state the expression of multiple co-stimulatory ligands and adhesion molecules that were described to play a role in DC-Treg interactions. We found that ICOS-L was significantly decreased at the surface of both *Atg5*^{-/-} DCs and *Atg14*^{-/-} DCs (Figures 3B and S3B). Interestingly, live cell imaging analysis confirmed that ICOS-L blocking on WT DCs significantly reduced the stability of their interaction with Tregs (Figure S3A). The central contribution of the ICOS-L pathway in Treg function and homeostasis has already been well established for populations of both natural Tregs and induced Tregs (iTregs) (Akbari et al., 2002). ICOS^{-/-} and ICOS-L^{-/-} animals have a defect in the pool size of Tregs (Burmeister et al., 2008), and blocking experiments have shown that the pathway contributes to the survival and function of effector Tregs (Raynor et al., 2015; Smigiel et al., 2014). However, while ICOS-L expression in plasmacytoid DCs was shown to contribute to Treg expansion and homeostasis (Conrad et al., 2012; Faget et al., 2012; Ito

et al., 2007), studies on the selective role of ICOS-L in conventional DCs (Teichmann et al., 2015) and its impact on Tregs are limited (Smigiel et al., 2014). Since ICOS-L is cleaved by ADAM10 metalloproteinase, we wondered if ICOS-L downregulation in *Atg5*^{-/-} DCs was related to ADAM10 accumulation. The surface expression of ADAM10 was significantly increased in *Atg5*^{-/-} DCs (Figure 3C), confirming, as recently reported in endothelial cells, that ADAM10 is a substrate of autophagosomal degradation (Maurer et al., 2015). Accordingly, the treatment of DCs with ADAM10 inhibitors significantly increased ICOS-L surface expression in *Atg5*^{-/-} DCs (Figure 3D). Because ICOS-L was also crucial in the priming of antigen-induced Tregs (Akbari et al., 2002), we confirmed *in vitro* that *Atg5*^{-/-} immature DCs prime significantly less iTregs in both a polyclonal set up and an epitope restricted manner (Figure 3E). These results extended our phenotype to the population of iTregs.

In Mice with Autophagy-Deficient DCs, Tregs Convert to Pathogenic Th17 and Exacerbate the Severity of Antigen-Induced Arthritis

Because the stability of Tregs is crucial during inflammation and autoimmunity, we wanted to assess the functional relevance of our phenotype *in vivo* in an inflammatory setting. We used the antigen-induced arthritis (AIA) model, a Th1/Th17 model of monoarthritis. We found no difference in joint swelling in the acute phase of arthritis (days 1–3), a stage that reflects the activation of the innate immune response (Figure S4A). This correlates with no differences in the expression of pro-inflammatory cytokines in the inflamed joints of *Atg5*^{-/-} DC mice, compared to their littermate controls (Figure S4B).

However, at a later time point (day 7), the severity of arthritis was significantly increased in *Atg5*^{-/-} DC mice, as assessed by histological scoring, showing enhanced synovial inflammation and increased cartilage and bone erosions (Figures 4A and 4B). In agreement with this phenotype, the Th1/Th17 response in *Atg5*^{-/-} DC mice was significantly higher (Figures 4C and S4C), while no differences in specific antibody titers were detected (Figure S4D). In addition, CD4⁺ T cells from draining LNs showed an increased proliferation in response to *in vitro* antigen re-stimulation (Figure S4E). This enhanced Th17 response could not be explained by an increase in cytokines responsible for Th17 priming (IL-1 β , IL-23, or IL-6) (Figure S4B). However, analysis of Tregs during AIA revealed a decrease in Foxp3 expression in *Atg5*^{-/-} DC mice, compared to their littermate controls, a phenotype that was not present in the steady state (Figure 4D). We therefore reasoned that Tregs in *Atg5*^{-/-} DC mice were unstable upon AIA and more prone to convert to Th17 cells, a possible mechanism leading to the increased severity of arthritis. To address this hypothesis, we used Tregs isolated from Foxp3-RFP/ROR γ t-GFP double-reporter mice. Since retinoic acid-related orphan receptor- γ t (ROR γ t) is a specific transcription factor for Th17 cell commitment, the conversion of Treg (RFP⁺GFP⁻) to Th17 (RFP⁺GFP⁺) cells could be easily tracked *in vivo* post transfer. When Tregs from Foxp3-RFP/ROR γ t-GFP mice were adoptively transferred 2 weeks prior to the induction of arthritis (Figures 4E and 4F), we only observed their conversion to Th17 cells in the inflamed knee of *Atg5*^{-/-} DC mice (RFP⁺GFP⁺), while in *Atg5*^{+/+}

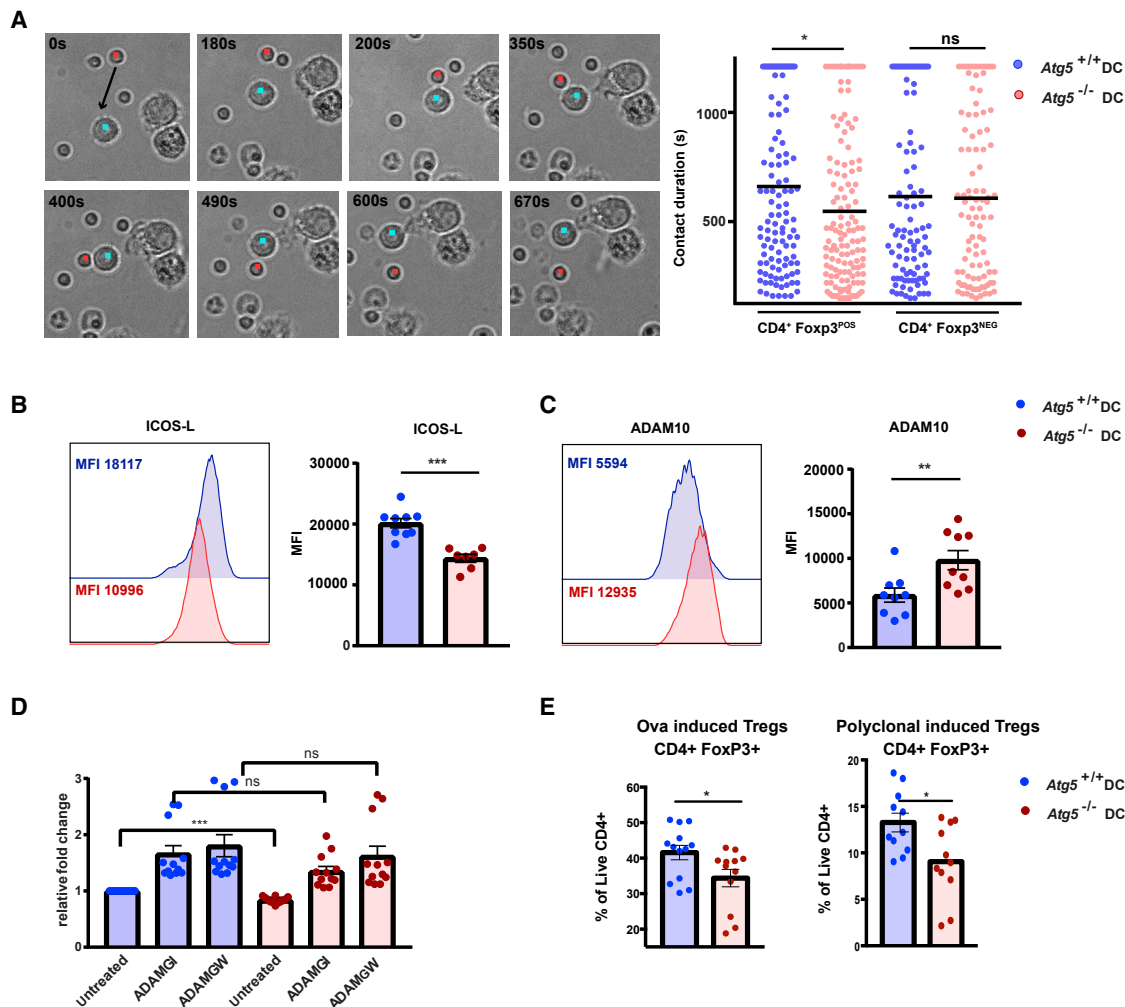


Figure 3. Autophagy Deficiency in DCs Alters DC-Treg Interactions and Reduces the Expression of ICOS-L

(A) Left: representative example of DC-T cell interaction: snapshots of live cell imaging data at indicated time points following a T cell (red dot) interacting with a DC (blue dot). Right: total interactions observed between CD4⁺ Foxp3^{NEG} T cells or CD4⁺ Foxp3^{POS} Tregs with immature *Atg5*^{+/+} or *Atg5*^{-/-} bone marrow derived dendritic cells (BMDCs). All T cells in the field of view were counted if they had contacted a DC for longer than 150 s. Data are from a combination of three individual experiments. Bar represents mean. *p < 0.05 (Mann-Whitney test).

(B and C) Representative histogram and flow cytometry analysis showing mean fluorescence intensity (MFI) of ICOS-L expression (B) and ADAM10 expression (C) in *Atg5*^{+/+} (blue) or *Atg5*^{-/-} (red) BMDC. Combination of 3–4 independent experiments with 1–3 technical replicates per experiment. Data shown represent mean ± SEM; *p < 0.05 (Mann-Whitney test).

(D) Flow cytometry analysis of ICOS-L expression from *Atg5*^{+/+} or *Atg5*^{-/-} BMDC treated with two ADAM10 inhibitors (GW280264X [GW] or GI254023X [GI]). Data shown represent the relative fold change of the ICOS-L MFI expression from *Atg5*^{+/+} DC untreated cells. Combination of three independent experiments with 3–4 technical replicates per experiment.

(E) Bar graphs showing CD4⁺ Foxp3⁺ expression from an *in vitro* induced Treg assay from OT-II naive sorted T cells (left) or CD4 polyclonal naive sorted T cells (right) co-cultured with ovalbumine (OVA) pulsed or control *Atg5*^{+/+} or *Atg5*^{-/-} BMDCs. Combined data from 3–4 independent experiments with 2–4 technical replicates per group. Data shown represent mean ± SEM; *p < 0.05 (Mann-Whitney test).

DC mice, expression of Foxp3 was sustained as RFP⁺GFP⁻ cells (Figure 4G).

Although we cannot rule out other additional mechanisms implicated in the exacerbation of arthritis, we have shown that Tregs convert to Th17 upon AIA in *Atg5*^{-/-} DC mice. Other studies have implicated autophagy in Tregs' function. In particular, Tregs were shown to inhibit the autophagic machinery in DCs in order to restrain their function (Alissafi et al., 2017). In parallel, the intrinsic conditional deletion of autophagy in Tregs was

shown to impair their function and integrity (Kabat et al., 2016; Wei et al., 2016).

Our data identify a mechanism where the autophagy pathway in DCs contributes to Tregs' stability and homeostasis in both steady state and inflammation. In the absence of autophagy in DCs, ICOS-L is downregulated as a consequence of ADAM10 accumulation, the metalloproteinase responsible for its cleavage. Accordingly, DC-Treg interactions are modified, resulting in Tregs' dysfunction and instability. Since genetic association

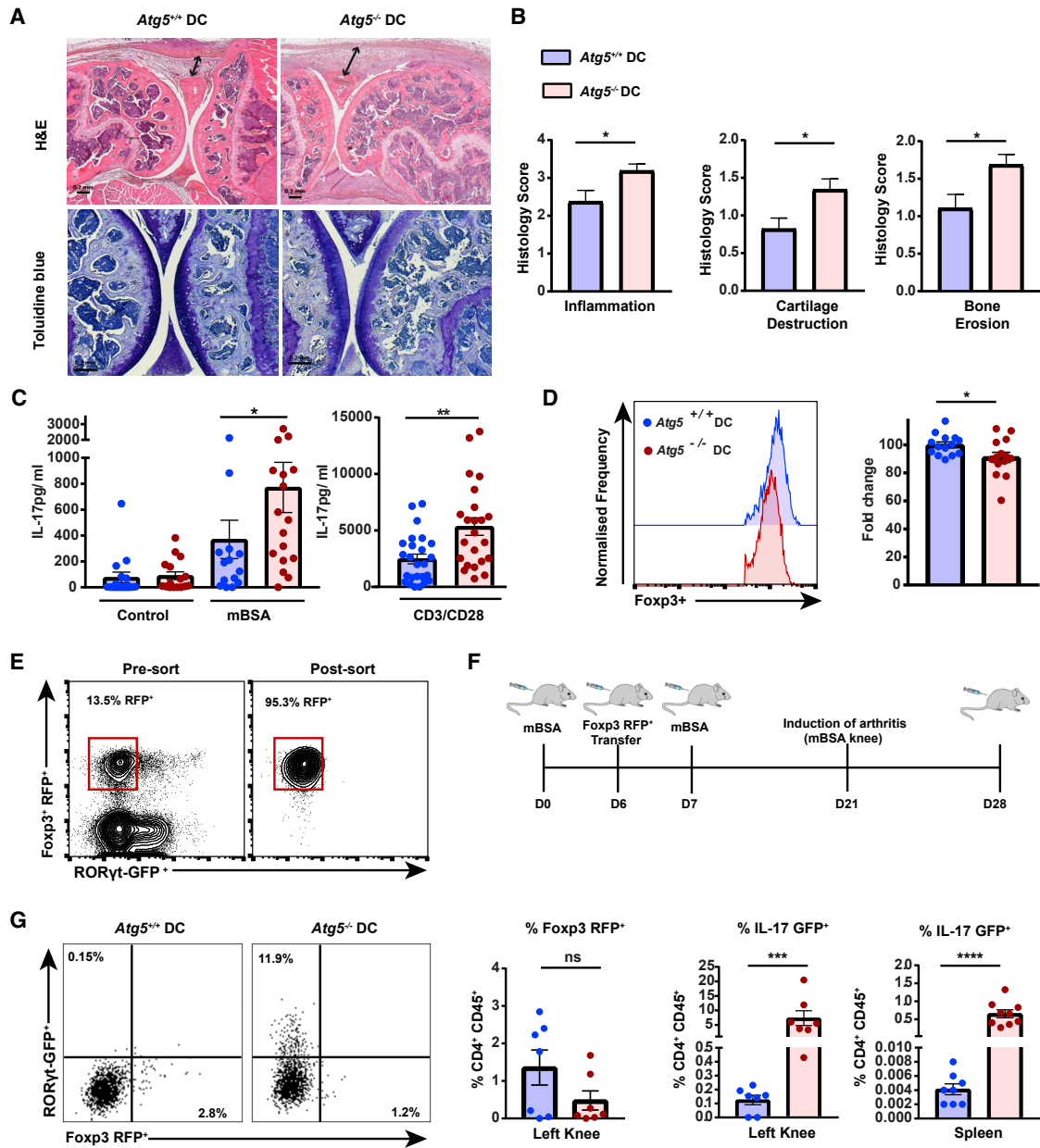


Figure 4. In Mice Lacking Autophagy in Their DCs, Tregs Convert to Pathogenic Th17 and Exacerbate Antigen-Induced Arthritis

(A) Representative histological sections of arthritic knee joints at d7 post-arthritis onset in *Atg5*^{+/+} DC or *Atg5*^{-/-} DC mice. Top: H&E staining. Arrows show synovial hyperplasia. Bottom: toluidine blue staining for articular cartilage analysis. Scale bars are depicted in the lower left of each histological section (0.2 mm)

(B) Combined histological scoring of two antigen-induced arthritis (AIA) experiments (n = 6–10 mice per group).

(C) IL-17 production from inguinal lymph node (LN) cell suspensions. T cells were stimulated with PBS, methylated BSA (mBSA), or CD3/CD28. Data are combined from 2 to 3 experiments with 8 to 10 mice per group.

(D) Representative FACS plots showing Foxp3⁺ expression within splenic CD4⁺ Foxp3⁺ cells during AIA at d5 and d7 post-arthritis induction (left). Bar graph shows the MFI fold change of Foxp3 expression *Atg5*^{-/-} DC mice compared to *Atg5*^{+/+} DC mice (right). Data are from a combination of two experiments with 5–9 mice per group.

(E) FACS plot showing the purity of RFP⁺-Foxp3⁺ Tregs isolated from Foxp3-RFP/RORγt-GFP double-reporter mice. Left: pre-sorted cells, gated within live CD4⁺ population. Right: post-sorted cells; RFP⁺ Foxp3⁺ purity is shown (>95% RFP⁺ Foxp3⁺).

(F) Outline of immunization time points in the AIA model with RFP⁺-Foxp3⁺ adoptive transfer.

(G) Flow cytometric analysis of Treg-to-Th17 conversion in the spleen and arthritic knees. Left: FACS plots showing GFP and RFP expression in the left knee (d7 post-arthritis induction). Cells are gated on live CD4⁺ CD45⁺ populations from the joints. Right: bar graphs showing the combined data from two independent experiments, with 3–4 mice per group. Data shown represent mean ± SEM. *p < 0.05; **p < 0.01; ***p < 0.001; ****p < 0.0001 (Mann-Whitney test).

studies have linked autophagy gene polymorphisms to autoimmune and inflammatory disorders, we propose that autophagy dysfunction in DCs could result in Treg instability and precipitate autoimmune disorders.

STAR★METHODS

Detailed methods are provided in the online version of this paper and include the following:

- **KEY RESOURCES TABLE**
- **LEAD CONTACT AND MATERIALS AVAILABILITY**
- **EXPERIMENTAL MODEL AND SUBJECT DETAILS**
 - Mice
 - Primary cells
- **METHOD DETAILS**
 - FACS analysis
 - FACS sorting
 - Induced Treg assay
 - Treg functional assay
 - T cell proliferation assay post-AIA
 - Quantitative RT-PCR (qPCR)
 - Western blot
- **QUANTIFICATION AND STATISTICAL ANALYSIS**
- **DATA AND CODE AVAILABILITY**
 - Data Resources

SUPPLEMENTAL INFORMATION

Supplemental Information can be found online at <https://doi.org/10.1016/j.celrep.2019.05.110>.

ACKNOWLEDGMENTS

We would like to thank Professor Walter Reith for his critical reading of the manuscript. We would like to thank Dr. Stefan Rose-John for his help and expertise on ADAM10 inhibition. We thank Pascale Sattouet for her help in the first step of this project, in particular in setting up the AIA model. We would like to thank Professor Cem Gabay (University of Geneva) and his team, especially Dominique Talabot and Gaby Palmer, for their help in the setup of the AIA model. We are grateful to Cecile Gameiro, Jean-Pierre Aubry-Lachainaye, and Gregory Schneider from the flow cytometry facility (University of Geneva) for their great help. We thank Céline Delucinge and Mylène Docquier from the Genomic Facility Center (University of Geneva) for their great help and expertise in analyzing and processing the data. M.G. is funded by the Institute of Rheumatology Research (Switzerland), the Swiss National Fund (310030_169938), and the Fondation de Reuter.

AUTHOR CONTRIBUTIONS

J.N. performed, conceived, and analyzed the experiments and wrote the manuscript. N.M. performed and analyzed the experiments. N.P. and S.L. analyzed RNA sequencing and performed GSEA. A.C. performed and analyzed western blotting experiments and assisted in all mouse experiments. G.H. assisted in mouse experiments. C.A.S. performed image analysis and scored AIA histological sections. S.H. conceived experiments and critically edited the manuscript. M.G. conceived, designed, and supervised the project and wrote the manuscript.

DECLARATION OF INTERESTS

The authors declare no competing interests.

Received: May 2, 2018

Revised: April 5, 2019

Accepted: May 29, 2019

Published: July 2, 2019

REFERENCES

- Akbari, O., Freeman, G.J., Meyer, E.H., Greenfield, E.A., Chang, T.T., Sharpe, A.H., Berry, G., DeKruyff, R.H., and Umetsu, D.T. (2002). Antigen-specific regulatory T cells develop via the ICOS-ICOS-ligand pathway and inhibit allergen-induced airway hyperreactivity. *Nat. Med.* **8**, 1024–1032.
- Alissafi, T., Banos, A., Boon, L., Sparwasser, T., Ghigo, A., Wing, K., Vassilopoulos, D., Boumpas, D., Chavakis, T., Cadwell, K., and Verginis, P. (2017). Tregs restrain dendritic cell autophagy to ameliorate autoimmunity. *J. Clin. Invest.* **127**, 2789–2804.
- Bailey-Bucktrout, S.L., Martinez-Llordella, M., Zhou, X., Anthony, B., Rosenthal, W., Luche, H., Fehling, H.J., and Bluestone, J.A. (2013). Self-antigen-driven activation induces instability of regulatory T cells during an inflammatory autoimmune response. *Immunity* **39**, 949–962.
- Bovenschen, H.J., van de Kerkhof, P.C., van Erp, P.E., Woestenenk, R., Joosten, I., and Koenen, H.J. (2011). Foxp3+ regulatory T cells of psoriasis patients easily differentiate into IL-17A-producing cells and are found in lesional skin. *J. Invest. Dermatol.* **131**, 1853–1860.
- Burmeister, Y., Lischke, T., Dahler, A.C., Mages, H.W., Lam, K.P., Coyle, A.J., Kroczeck, R.A., and Hutloff, A. (2008). ICOS controls the pool size of effector-memory and regulatory T cells. *J. Immunol.* **180**, 774–782.
- Camps, M., Rückle, T., Ji, H., Ardisson, V., Rintelen, F., Shaw, J., Ferrandi, C., Chabert, C., Gillieron, C., Françon, B., et al. (2005). Blockade of PI3Kgamma suppresses joint inflammation and damage in mouse models of rheumatoid arthritis. *Nat. Med.* **11**, 936–943.
- Chen, Z., Barbi, J., Bu, S., Yang, H.Y., Li, Z., Gao, Y., Jinasena, D., Fu, J., Lin, F., Chen, C., et al. (2013). The ubiquitin ligase Stub1 negatively modulates regulatory T cell suppressive activity by promoting degradation of the transcription factor Foxp3. *Immunity* **39**, 272–285.
- Chinen, T., Kannan, A.K., Levine, A.G., Fan, X., Klein, U., Zheng, Y., Gasteiger, G., Feng, Y., Fontenot, J.D., and Rudensky, A.Y. (2016). An essential role for the IL-2 receptor in T_{reg} cell function. *Nat. Immunol.* **17**, 1322–1333.
- Conrad, C., Gregorio, J., Wang, Y.H., Ito, T., Meller, S., Hanabuchi, S., Anderson, S., Atkinson, N., Ramirez, P.T., Liu, Y.J., et al. (2012). Plasmacytoid dendritic cells promote immunosuppression in ovarian cancer via ICOS costimulation of Foxp3(+) T-regulatory cells. *Cancer Res.* **72**, 5240–5249.
- Darrasse-Jèze, G., Deroubaix, S., Mouquet, H., Vitorica, G.D., Eisenreich, T., Yao, K.H., Masilamani, R.F., Dustin, M.L., Rudensky, A., Liu, K., and Nussenzweig, M.C. (2009). Feedback control of regulatory T cell homeostasis by dendritic cells in vivo. *J. Exp. Med.* **206**, 1853–1862.
- Delpoux, A., Yakonowsky, P., Durand, A., Charvet, C., Valente, M., Pommier, A., Bonilla, N., Martin, B., Auffray, C., and Lucas, B. (2014). TCR signaling events are required for maintaining CD4 regulatory T cell numbers and suppressive capacities in the periphery. *J. Immunol.* **193**, 5914–5923.
- Deretic, V., Saitoh, T., and Akira, S. (2013). Autophagy in infection, inflammation and immunity. *Nat. Rev. Immunol.* **13**, 722–737.
- Dobin, A., Davis, C.A., Schlesinger, F., Drenkow, J., Zaleski, C., Jha, S., Batut, P., Chaisson, M., and Gingeras, T.R. (2013). STAR: ultrafast universal RNA-seq aligner. *Bioinformatics* **29**, 15–21.
- Duarte, J.H., Zelenay, S., Bergman, M.L., Martins, A.C., and Demengeot, J. (2009). Natural Treg cells spontaneously differentiate into pathogenic helper cells in lymphopenic conditions. *Eur. J. Immunol.* **39**, 948–955.
- Faget, J., Bendriss-Vermare, N., Gobert, M., Durand, I., Olive, D., Biota, C., Bachelot, T., Treilleux, I., Goddard-Leon, S., Lavergne, E., et al. (2012). ICOS-ligand expression on plasmacytoid dendritic cells supports breast cancer progression by promoting the accumulation of immunosuppressive CD4+ T cells. *Cancer Res.* **72**, 6130–6141.

- Feng, Y., Arvey, A., Chinen, T., van der Veecken, J., Gasteiger, G., and Rudensky, A.Y. (2014). Control of the inheritance of regulatory T cell identity by a cis element in the Foxp3 locus. *Cell* 158, 749–763.
- Fontenot, J.D., Gavin, M.A., and Rudensky, A.Y. (2003). Foxp3 programs the development and function of CD4+CD25+ regulatory T cells. *Nat. Immunol.* 4, 330–336.
- Fontenot, J.D., Rasmussen, J.P., Williams, L.M., Dooley, J.L., Farr, A.G., and Rudensky, A.Y. (2005). Regulatory T cell lineage specification by the forkhead transcription factor foxp3. *Immunity* 22, 329–341.
- Gabryšová, L., Christensen, J.R., Wu, X., Kissenpfennig, A., Malissen, B., and O'Garra, A. (2011). Integrated T-cell receptor and costimulatory signals determine TGF- β -dependent differentiation and maintenance of Foxp3+ regulatory T cells. *Eur. J. Immunol.* 41, 1242–1248.
- Hara, T., Nakamura, K., Matsui, M., Yamamoto, A., Nakahara, Y., Suzuki-Migishima, R., Yokoyama, M., Mishima, K., Saito, I., Okano, H., and Mizushima, N. (2006). Suppression of basal autophagy in neural cells causes neurodegenerative disease in mice. *Nature* 441, 885–889.
- Hoffmann, P., Boeld, T.J., Eder, R., Huehn, J., Floess, S., Wieczorek, G., Olek, S., Dietmaier, W., Andreesen, R., and Edinger, M. (2009). Loss of FOXP3 expression in natural human CD4+CD25+ regulatory T cells upon repetitive in vitro stimulation. *Eur. J. Immunol.* 39, 1088–1097.
- Hubbard-Lucey, V.M., Shono, Y., Maurer, K., West, M.L., Singer, N.V., Ziegler, C.G., Lezcano, C., Motta, A.C., Schmid, K., Levi, S.M., et al. (2014). Autophagy gene Atg16L1 prevents lethal T cell alloreactivity mediated by dendritic cells. *Immunity* 41, 579–591.
- Ito, T., Yang, M., Wang, Y.H., Lande, R., Gregorio, J., Perng, O.A., Qin, X.F., Liu, Y.J., and Gilliet, M. (2007). Plasmacytoid dendritic cells prime IL-10-producing T regulatory cells by inducible costimulator ligand. *J. Exp. Med.* 204, 105–115.
- Josefowicz, S.Z., Lu, L.F., and Rudensky, A.Y. (2012). Regulatory T cells: mechanisms of differentiation and function. *Annu. Rev. Immunol.* 30, 531–564.
- Kabat, A.M., Harrison, O.J., Riffelmacher, T., Moghaddam, A.E., Pearson, C.F., Laing, A., Abeler-Dörner, L., Forman, S.P., Grecis, R.K., Sattentau, Q., et al. (2016). The autophagy gene Atg16l1 differentially regulates Treg and TH2 cells to control intestinal inflammation. *eLife* 5, e12444.
- Kim, J.M., Rasmussen, J.P., and Rudensky, A.Y. (2007). Regulatory T cells prevent catastrophic autoimmunity throughout the lifespan of mice. *Nat. Immunol.* 8, 191–197.
- Koenen, H.J., Smeets, R.L., Vink, P.M., van Rijssen, E., Boots, A.M., and Joosten, I. (2008). Human CD25highFoxp3pos regulatory T cells differentiate into IL-17-producing cells. *Blood* 112, 2340–2352.
- Komatsu, N., Mariotti-Ferrandiz, M.E., Wang, Y., Malissen, B., Waldmann, H., and Hori, S. (2009). Heterogeneity of natural Foxp3+ T cells: a committed regulatory T-cell lineage and an uncommitted minor population retaining plasticity. *Proc. Natl. Acad. Sci. USA* 106, 1903–1908.
- Komatsu, N., Okamoto, K., Sawa, S., Nakashima, T., Oh-hora, M., Kodama, T., Tanaka, S., Bluestone, J.A., and Takayanagi, H. (2014). Pathogenic conversion of Foxp3+ T cells into TH17 cells in autoimmune arthritis. *Nat. Med.* 20, 62–68.
- Levine, A.G., Arvey, A., Jin, W., and Rudensky, A.Y. (2014). Continuous requirement for the TCR in regulatory T cell function. *Nat. Immunol.* 15, 1070–1078.
- Li, X., Liang, Y., LeBlanc, M., Benner, C., and Zheng, Y. (2014). Function of a Foxp3 cis-element in protecting regulatory T cell identity. *Cell* 158, 734–748.
- Liu, Z., Germer, M.Y., Van Panhuys, N., Levine, A.G., Rudensky, A.Y., and Germain, R.N. (2015). Immune homeostasis enforced by co-localized effector and regulatory T cells. *Nature* 528, 225–230.
- Long, S.A., Cerasoletti, K., Bollyky, P.L., Tatum, M., Shilling, H., Zhang, S., Zhang, Z.Y., Pihoker, C., Sanda, S., Greenbaum, C., and Buckner, J.H. (2010). Defects in IL-2R signaling contribute to diminished maintenance of FOXP3 expression in CD4+CD25(+) regulatory T-cells of type 1 diabetic subjects. *Diabetes* 59, 407–415.
- Maurer, K., Reyes-Robles, T., Alonzo, F., 3rd, Durbin, J., Torres, V.J., and Cadwell, K. (2015). Autophagy mediates tolerance to Staphylococcus aureus alpha-toxin. *Cell Host Microbe* 17, 429–440.
- Miyao, T., Floess, S., Setoguchi, R., Luche, H., Fehling, H.J., Waldmann, H., Huehn, J., and Hori, S. (2012). Plasticity of Foxp3(+) T cells reflects promiscuous Foxp3 expression in conventional T cells but not reprogramming of regulatory T cells. *Immunity* 36, 262–275.
- Overacre-Delgoffe, A.E., Chikina, M., Dadey, R.E., Yano, H., Brunazzi, E.A., Shayan, G., Horne, W., Moskovitz, J.M., Kolls, J.K., Sander, C., et al. (2017). Interferon-gamma Drives Treg Fragility to Promote Anti-tumor Immunity. *Cell* 169, 1130–1141.e1111.
- Quinlan, A.R., and Hall, I.M. (2010). BEDTools: a flexible suite of utilities for comparing genomic features. *Bioinformatics* 26, 841–842.
- Raynor, J., Karns, R., Almanan, M., Li, K.P., Divanovic, S., Chouhnet, C.A., and Hildeman, D.A. (2015). IL-6 and ICOS Antagonize Bim and Promote Regulatory T Cell Accrual with Age. *J. Immunol.* 195, 944–952.
- Redpath, S.A., van der Werf, N., Cervera, A.M., MacDonald, A.S., Gray, D., Maizels, R.M., and Taylor, M.D. (2013). ICOS controls Foxp3(+) regulatory T-cell expansion, maintenance and IL-10 production during helminth infection. *Eur. J. Immunol.* 43, 705–715.
- Robinson, M.D., McCarthy, D.J., and Smyth, G.K. (2010). edgeR: a Bioconductor package for differential expression analysis of digital gene expression data. *Bioinformatics* 26, 139–140.
- Sarris, M., Andersen, K.G., Randow, F., Mayr, L., and Betz, A.G. (2008). Neurophilin-1 expression on regulatory T cells enhances their interactions with dendritic cells during antigen recognition. *Immunity* 28, 402–413.
- Schmid, D., Pypaert, M., and Münz, C. (2007). Antigen-loading compartments for major histocompatibility complex class II molecules continuously receive input from autophagosomes. *Immunity* 26, 79–92.
- Smigielski, K.S., Richards, E., Srivastava, S., Thomas, K.R., Dudda, J.C., Klonowski, K.D., and Campbell, D.J. (2014). CCR7 provides localized access to IL-2 and defines homeostatically distinct regulatory T cell subsets. *J. Exp. Med.* 211, 121–136.
- Teichmann, L.L., Cullen, J.L., Kashgarian, M., Dong, C., Craft, J., and Shlomchik, M.J. (2015). Local triggering of the ICOS coreceptor by CD11c(+) myeloid cells drives organ inflammation in lupus. *Immunity* 42, 552–565.
- Valencia, X., Stephens, G., Goldbach-Mansky, R., Wilson, M., Shevach, E.M., and Lipsky, P.E. (2006). TNF downmodulates the function of human CD4+CD25hi T-regulatory cells. *Blood* 108, 253–261.
- Wei, J., Long, L., Yang, K., Guy, C., Shrestha, S., Chen, Z., Wu, C., Vogel, P., Neale, G., Green, D.R., and Chi, H. (2016). Autophagy enforces functional integrity of regulatory T cells by coupling environmental cues and metabolic homeostasis. *Nat. Immunol.* 17, 277–285.
- Xu, L., Kitani, A., Fuss, I., and Strober, W. (2007). Cutting edge: regulatory T cells induce CD4+CD25-Foxp3- T cells or are self-induced to become Th17 cells in the absence of exogenous TGF-beta. *J. Immunol.* 178, 6725–6729.
- Zhou, X., Bailey-Bucktrout, S.L., Jeker, L.T., Penaranda, C., Martínez-Llorca, M., Ashby, M., Nakayama, M., Rosenthal, W., and Bluestone, J.A. (2009). Instability of the transcription factor Foxp3 leads to the generation of pathogenic memory T cells in vivo. *Nat. Immunol.* 10, 1000–1007.

STAR★METHODS

KEY RESOURCES TABLE

REAGENT or RESOURCE	SOURCE	IDENTIFIER
Antibodies		
Pacific Blue anti-mouse CD4 (RM4-5)	BioLegend	Cat#100531; RRID:AB_493374
APC-Cy7 anti-mouse CD44 (IM7)	BioLegend	Cat#103027; RRID:AB_830784
PE-Cy7 anti-mouse CD62L (MEL-14)	BioLegend	Cat#104418; RRID:AB_313103
APC anti-mouse CD25 (PC61),	BioLegend	Cat#102012; RRID:AB_312861
PE-CY7 anti-mouse CD45.1 (A20)	BioLegend	Cat#110730; RRID:AB_1134168
APC-CY7 anti-mouse CD45.2 (104)	BioLegend	Cat#109824; RRID:AB_830789
FITC anti-mouse CD103 (2E7)	BioLegend	Cat#121419; RRID:AB_10709438
FITC anti-mouse CD69 (H1.2F3)	BioLegend	Cat#104505; RRID:AB_313108
BV421 anti-mouse ICOS (7E.17G9)	BD Biosciences	Cat#564070; RRID:AB_2738576
PE-CY7 anti-mouse CD11c (N418)	BioLegend	Cat#117318; RRID:AB_493568
ALEXA 647 anti-mouse MHCII /I-Ab (AF6-120.1)	BioLegend	Cat#116412; RRID:AB_493141
PE-Cy7 Ki67 (SolA15)	ebioscience - ThermoFisher Scientific	Cat#25-5698-82; RRID:AB_11220070
PE anti- mouse/rat Foxp3 (FJK-16 s)	ebioscience - ThermoFisher Scientific	Cat#12-5773-82; RRID:AB_465936
PE anti-mouse ICOS L (HK-5.3)	BioLegend	Cat#107405; RRID:AB_2248797
PE anti-mouse CD80 (16-10A1)	ebioscience - ThermoFisher Scientific	Cat#12-0801-82; RRID:AB_465752
Percp/Cy5.5 anti-mouse CD86 (GL-1)	BioLegend	Cat#105028; RRID:AB_2074994
APC anti-mouse CD40 (HM40-3)	ebioscience - ThermoFisher Scientific	Cat#17-0402-82; RRID:AB_10853008
PE- anti- mouse/human Semaphorine 4a (5E3)	BioLegend	Cat#148404; RRID:AB_2565287
Purified anti-mouse CD3e	BioLegend	Cat#100302; RRID:AB_312667
Purified anti-mouse CD28	BioLegend	Cat#102102; RRID:AB_312867
Purified anti-mouse CD3e	Bio X Cell	Cat#BE0001
Purified anti-mouse CD28	Bio X Cell	Cat#BE0015
TruStain fcX anti-CD16/32	BioLegend	Cat#101320; RRID:AB_1574975
LEAF Purified anti-mouse ICOS Ligand	BioLegend	Cat# 107408; RRID:AB_2122716
LEAF Purified Rat IgG2a, κ Isotype Ctrl	BioLegend	Cat# 400533
Rat Anti-Mouse Adam-10 purified (139712)	R and D Systems	Cat#MAB946; RRID:AB_2222927
Anti-HSPA1A	Sigma-Aldrich	Cat#SAB2700846
Goat Anti-Rabbit IgG (H+L)-HRP conjugate	Bio-Rad	Cat#1706515 RRID:AB_11125142
Goat Anti-Mouse IgG (H + L)-HRP	Bio-Rad	Cat#1706516 RRID:AB_11125547
Chemicals, Peptides, and Recombinant Proteins		
LIVE/DEAD Fixable aqua stain kit	Invitrogen - ThermoFisher Scientific	Cat#L34957
LIVE/DEAD Fixable NEAR-IR stain kit	Invitrogen - ThermoFisher Scientific	Cat#L10119
Recombinant mouse GM-CSF	PeproTech	Cat#315-03
Cell trace CFSE cell proliferation kit	Invitrogen - ThermoFisher Scientific	Cat#C34554
Cell trace violet cell proliferation kit	Invitrogen - ThermoFisher Scientific	Cat#C34557
Recombinant human IL-2	Peprtech	Cat#200-02
ADAM inhibitor GI254023X	Sigma-Aldrich	Cat#SML0789
ADAM inhibitor GW280264X	Aobious	Cat#AOB3632
Collagenase D	Roche-Sigma-Aldrich	Cat#11088858001
DNase	Sigma-Aldrich	Cat#1010415900
HEPES buffer	GIBCO - ThermoFisher Scientific	Cat#15630056
Recombinant human TFG-β	eBioscience - ThermoFisher Scientific	Cat#14-8348

(Continued on next page)

Continued

REAGENT or RESOURCE	SOURCE	IDENTIFIER
OVA specific peptide (OVA 323-339)	InvivoGen	Cat#Vac-isq
Lipopolysaccharides from <i>Escherichia coli</i> O55:B5	Sigma-Aldrich	Cat#L2880
Methylated bovine serum albumin	Sigma-Aldrich	Cat#A1009
Complete Freund's adjuvant	Chondrex - Amsbio	Cat#7001
Incomplete Freund's adjuvant	Chondrex - Amsbio	Cat#7002
Critical Commercial Assays		
RNeasy Mini kit	QIAGEN	Cat#74104
IL-17 ELISA	ebioscience –ThermoFisher Scientific	Cat#88-7371-88
IFN γ ELISA	ebioscience –ThermoFisher Scientific	Cat# 88-7314-88
EasySep Mouse CD4+ T Cell Isolation Kit	Stem Cell Technologies	Cat#19752
CD11c MicroBeads UltraPure, mouse	Miltenyi Biotec	Cat#130-108-338
Deposited Data		
RNA sequencing data	This study	GEO: GSE98961
Experimental Models: Organisms/Strains		
Atg5 ^{flox/flox}	Pr Noburu Mizushima (Tokyo, Japan)	MTA
CD11c-Cre Tg	The Jackson Laboratory	Cat#007567
Foxp3 ^{RFP} ROR γ t ^{GFP}	Dr Mathias Lochner, Hannover Medical school	
C57BL/6 CD45.1	Charles River Laboratories	Cat#494
C57BL/6 OT II	The Jackson Laboratory	Cat#004194
Atg14 ^{flox/flox}	Pr Shizuo Akira (Osaka, Japan)	MTA 17-059
Oligonucleotides		
Primer: IL-6 forward: GCTACCAAAGTGGATATAA TCAGGA	This paper	N/A
Primer: IL-6 reverse: GCTACCAAAGTGGATAT AATCAGGA	This paper	N/A
Primer: IL-1 β forward AGTTGACGGACCCAAAAG	This paper	N/A
Primer: IL-1 β reverse AGCTGGATGCTCTCATCAGG	This paper	N/A
Primer: IL-23 forward TCCCTACTAGGACTCA GCCAAC	This paper	N/A
Primer: IL-23 reverse AGAACTCAGGCTGGGCATC	This paper	N/A
Primer: GAPDH forward ACGGCCGCATCTTC TTGTGCA	This paper	N/A
Primer: GAPDH reverse AATGGCAGCCCT GGTGACCA	This paper	N/A
Software and Algorithms		
Flow Jo Version 10. software (Treestar)	Treestar Inc	N/A
Kalusa analysis software (version1.3)	Beckman Coulter	N/A
Prism 7	Graphpad Inc	
ImageJ	National Institute of Health, available online	N/A

LEAD CONTACT AND MATERIALS AVAILABILITY

Further information and requests for resources and reagents should be directed to and will be fulfilled by the Lead Contact, Monique Gannagé: Monique.ghannage@chuv.ch.

EXPERIMENTAL MODEL AND SUBJECT DETAILS

Mice

Mice strains used in this study are: CD45.1(Charles River, France), C57BL/6 (Janvier), $Atg5^{flox/flox}$ (Hara et al., 2006) (Pr Mizushima, Tokyo, Japan), CD11c-Cre Tg (Jackson Laboratory), $Atg14^{flox/flox}$ (Pr Akira, Osaka Japan), OT-II (Charles River Laboratory), $Foxp3^{RFP}$ $ROR\gamma^{GFP}$ (Mathias Lochner, Hannover Medical School). $Atg5^{-/-}$ DC mice ($Atg5^{flox/flox}$ -CD11-Cre^{+/-}) and $Atg5^{+/+}$ DC ($Atg5^{flox/flox}$ -CD11-Cre^{-/-}) mice were obtained by crossing $Atg5^{flox/flox}$ mice to CD11-Cre^{+/-} mice. Animals were crossed, bred and housed under specific-pathogen-free conditions in the animal facility of the faculty of Medicine, University of Geneva, Switzerland. Male and female mice ranging from 8-14 weeks of age were used in experiments. Animals were aged and sex matched and assigned to experimental groups, using littermate controls. All animal protocols were approved by the cantonal veterinary office of the canton of Geneva, Switzerland (authorization number GE/103/18 and GE/38/14 and FRM1005-Medicine CMU).

Primary cells

Bone marrow derived dendritic cells (BMDCs)

Bone marrow cells were isolated from tibias and femurs from $Atg5^{+/+}$ DC and $Atg5^{-/-}$ DC mice. Cells were expanded using X63 cell supernatant as a source of GM-CSF or recombinant GM-CSF (20ng/ml) in culture medium. GM-CSF supplemented media was replaced every three days. Cells were used at Day 10 of culture. For functional assay, to ensure a pure DC population of > 90% CD11c⁺ MHCII⁺, cells were enriched by CD11c⁺ selection (Miltenyi).

Splenic DCs

Splenocytes from $Atg5^{+/+}$ DC or $Atg5^{-/-}$ DC mice were digested using 0.2mg/ml Collagenase D (Roche), 25ug/ml DNase (Sigma) and 25mM HERPES (GIBCO) for 30 min at 37°C. After red blood cell lysis, the single cell splenocytes suspension obtained underwent FACS staining or was enriched by CD11c⁺ selection (Miltenyi) before FACS sorting.

METHOD DETAILS

FACS analysis

For staining, the following Abs were purchased from Biolegend BD Bioscience, or ebioscience (unless otherwise stated) as conjugated to FITC, PE, PE-CF 594, PE-Cy7, PerCP-Cy5.5, APC, APC-Cy7, Alexa Fluor 700, Pacific Blue: anti-CD4 (RM4-5), CD44 (IM7), CD62L (MEL-14), CD25 (PC61), CD45.1 (A20), CD45.2 (104), CD103 (2E7), CD69 (H1.2F3), ICOS (7E.17G9), CD11c (N418), MHCII /I-Ab (AF6-120.1), Ki67 (SolA15, eBioscience), Foxp3 (FJK-16 s), ICOS L (HK-5.3), CD80 (16-10A1), CD86 (GL-1), CD40 (HM40-3), Semaphorin 4a (5E3), CD308 (3DS304M). For ADAM10 expression, cells were first stained with Anti-rat ADAM10 (purified Rat-monoclonal, clone 139712, R&D systems), followed by an Anti-Rat PE conjugated secondary antibody (Jackson). For dead cell exclusion, LIVE/DEAD[®] fixable Aqua or Near-IR kit (Invitrogen) was used. Cells were acquired on a Gallios flow cytometer (Beckman Coulter), or on an LSR Fortessa (BD Bioscience). All flow cytometry analysis were performed using Flow Jo Version 10. software (TreeStar) or Kalusa analysis software (version1.3).

FACS sorting

For Treg isolation, CD4⁺ T cell populations, from LN and spleens were selected by a CD4 negative selection kit (Stem Cell Technologies). After the CD4⁺ enrichment, cells were labeled with the specific Abs, as follow: for isolation of CD25^{High/Low} T reg populations, CD4⁺ CD62L^{High} (CD44^{Low}) CD25^{High} or CD4⁺ CD62L^{High} (CD44^{Low}) CD25^{Low} or CD4⁺ CD62L^{High} (CD44^{Low}) total CD25⁺ were isolated. Post-sort analysis of Treg purity was assessed by FACS by Foxp3 staining (purity between 95 and 97%).

For Treg adoptive transfer experiments, CD4⁺ RFP⁺ cells were isolated from $Foxp3^{RFP}$ $ROR\gamma^{GFP}$ mice.

For CD4⁺ Naive T cells isolation, CD4⁺ T cell populations from LN and spleens were selected by a CD4 negative selection kit (Stem Cell Technologies). CD4⁺ CD62L^{High} CD44^{Low} CD25^{Neg} were FACS sorted.

For Treg adoptive transfer to CD45.1 OT-II mice, Tregs (CD4⁺ CD62L⁺ CD25⁺) were FACS sorted from $Atg5^{+/+}$ DC or $Atg5^{-/-}$ DC mice and stained with cell trace violet (Invitrogen).

For DC isolation, Splenic DCs were FACS sorted as CD11c^{High} MHC class II^{High}.

All cells were sorted on a Beckman Coulter MoFlo Astrios or a Biorad S3 sorter.

Induced Treg assay

BMDCs from $Atg5^{+/+}$ or $Atg5^{-/-}$ mice were obtained as previous described. For polyclonal Tregs induction: Naive T cells from CD45.1 cells were isolated by FACS sorting. 1×10^5 T cells were co cultured with 1×10^5 $Atg5^{+/+}$ or $Atg5^{-/-}$ BMDC in the presence of 500 U/ml IL-2 and 20ng/ml TFG- β . Cytokines were replaced at day 3 of culture and cells isolated on day 5 for analysis CD4⁺ Foxp3⁺ expression by flow cytometry. For OVA specific Tregs induction: Naive T cells were isolated from OT-II TCR mice and co-cultured with BMDC which had undergone pulsing with 0.1ug/ml OVA specific peptide (OVA peptide 323-339, InvivoGen) for 2h at 37°C. Cells were then washed before the co-culture.

Treg functional assay

To determine the suppression capacity of Tregs *in vitro*, FACS sorted T regs from *Atg5^{+/+}* DC or *Atg5^{-/-}* DC mice were co-cultured with FACS sorted Naive CD45.1 cells which were labeled with cell trace violet (Invitrogen), in the presence of FACS sorted splenic DCs. Treg: T naive cells were cultured in RPMI supplemented with 10% FCS, 1% p/s and 2×10^5 M β -2 mercapto-ethanol at varying ratios, with 0.2 μ g/ml of anti-CD3 (Biolegend). After 5 days, proliferation of effector cells was assessed by the loss of cell trace violet expression on CD4⁺ CD45.1⁺ by flow cytometry.

ADAM inhibition for ICOSL regulation

BMDC from *Atg5^{+/+}* or *Atg5^{-/-}* mice were obtained as previous described. At day 10 of culture, 0.5×10^6 cells were seeded in a 12 well plate in complete medium supplemented with 20ng/ml GM-CSF. Cells were then treated for 24h with 3μ M ADAM inhibitor GI254023X (Sigma) or GW280264X (Aobious). The expression of ICOS-L was then assessed by flow cytometry.

Antigen Induced Arthritis (AIA) model

Mice were immunized subcutaneously at the base of the tail with 100ug methylated bovine serum albumin (mBSA) (Sigma) emulsified in complete Freund's adjuvant (CFA) (Chondrex). On day 7, mice underwent a boost injection of 100ug mBSA emulsified with incomplete Freund's adjuvant (Chondrex). Arthritis was induced on day 21 by intra-articular injection of 100ug mBSA into the left knee joint, PBS was injected into the right knee joint. Joint swelling was evaluated by measuring ^{99m}Tc uptake, on day 1 and day 3 post injection. Briefly, ^{99m}Tc, mice was injected subcutaneously in the neck, and after 30 min knee joint were placed on a gamma counter. The ratio of ^{99m}Tc up take in the inflamed joint was calculated as compared to the PBS control joint. Mice were sacrificed at day 28 unless otherwise stated.

Histological analysis of AIA

At day 28 post AIA induction, mice were sacrificed and knee joints were fixed in 10% buffered formalin, decalcified in 10% EDTA, and embedded in paraffin. Sections were stained with hematoxylin and eosin or toluidine blue and graded by one pathologist (CAS) in a blinded manner. The severity of the synovial inflammation including synovial hyperlasia and the % of neutrophil cell infiltration, as well as the degree of cartilage and bone erosion were evaluated utilizing a scoring system (Camps et al., 2005) ranging from 0 to 4 (0 = normal, 1 = minimal, 2 = moderate, 3 = severe, 4 = very severe).

T cell proliferation assay post-AIA

To assess T cell proliferation, lymph node cell suspensions taken at day 7 post arthritis induction were labeled with carboxy-fluorescein diacetate succin-imidyl ester (CFSE) and treated *ex vivo* with 10 μ g/ml mBSA or 2.5 μ g/ml CD3/CD28 (Biolegend), and cultured in RPMI supplemented with 10% FCS, 1% p/s and 2×10^5 M β -2 mercapto-ethanol. After 72h, cells were harvested and proliferation assessed by loss of CFSE staining by flow cytometry.

ELISA Assay

For detection of cytokines production from T cells during AIA, single cell suspensions were prepared from lymph nodes taken at day 7 post arthritis induction and treated *ex vivo* with 10 μ g/ml mBSA or 2.5 μ g/ml CD3/CD28 (Biolegend), and cultured in RPMI supplemented with 10% FCS, 1% p/s and 2×10^5 M β -2 mercapto-ethanol. After 72h supernatants were tested for IL-17 and IFN γ cytokine production by ELISA according to manufacturer's specifications (e.Bioscience).

For anti-mBSA IgG antibody levels: To assess anti-mBSA specific antibody production during AIA, serum was collected from arthritic mice at day 7 post arthritis induction. mBSA (Sigma), at 10ug/ml was coated on 96 well plates (Nunc) overnight at 4°C in PBS. After multiple washes with 0.05% PBS Tween, serum was serially diluted and incubated with HRP-conjugated antibody for murine total IgG, IgG2A or IgG1. The plates were then washed and incubated with 3,3',5,5'-Tetramethylbenzidine (TMB) substrate. Antibody titers were determined by taking the last positive OD readout above the background. The background was determined by the OD values from the serum of mouse injected with CFA only.

Treg adoptive transfer upon AIA

To determine the conversion of Foxp3-RFP^{POS} to Rorc γ t-GFP^{POS} during AIA, RFP^{POS}GFP^{neg} cells were isolated by FACS and injected IV at day 6 post immunisation. Knee joints were isolated at day 28 (21 days post transfer), and single cell suspensions of knee joints were achieved after knee digestion (0.2mg/ml collagenase A) and Percoll density centrifugation. Foxp3 RFP^{POS} and Rorc γ t GFP^{POS} cells were identified by flow cytometry. Background GFP⁺ or RFP⁺ was determined from non-injected control mice (3 mice per phenotype). For the analysis of Tregs in the knee, all GFP⁺ values < 1% and Foxp3 RFP⁺ values < 0.6% were considered as background. Mice having a minimum of 450 CD4⁺ CD45⁺ cells in the live gate were included in FACS analysis. According to rare event analysis the precision of our data was lower or equal to 20% (as calculated by $n^{1/2}$ where n is the total numbers of cells, in the live gate). For the analysis of splenic Tregs, all GFP⁺ values < 0.3% and Foxp3 RFP⁺ values < 0.07% were considered as background

Quantitative RT-PCR (qPCR)

At day 4 post arthritis induction, knee joints from mBSA treated or PBS control were snap frozen. Total RNA was extracted using TRIzol (Invitrogen) and RNeasy mini columns with DNase digestion, according to manufacturer's instructions (QIAGEN). Reverse transcription was preformed using Superscript II (Invitrogen). The RT product was diluted and used as a template for quantitative PCR (qPCR) on a CFX Connect real-time detection system (Biorad) using kappa SYBR Green (Kappa Biosystems). The following specific forward and reverse primers (Microsynth) were used:

IL-6 forward 5' GCTACCAAAGTGGATATAATCAGGA 3'
 IL-6 reverse 5'CCAGGTAGCTATGGTACTCCAGAA 3'.
 IL-1 β forward 5'AGTTGACGGACCCCAAAAG 3'
 IL-1 β reverse 5' AGCTGGATGCTCTCATCAGG 3'
 IL-23 forward 5' TCCCTACTAGGACTCAGCCAAC3'
 IL-23 reverse 5' AGAACTCAGGCTGGGCATC 3'.
 GAPDH forward 5' ACGGCCGCATCTTCTTGTCAG3'
 GAPDH reverse 5' AATGGCAGCCCTGGTGACCA 3'

Relative fold change of gene expression was determined by analysis of the cycle threshold values (CT), and normalized to the expression of the GAPDH (delta CT).

The delta delta CT was then calculated taking the delta CT mean of PBS treated control knee joint in *Atg5^{+/+}* DC mice as a reference. The fold change of expression in the inflamed knee was calculated as $(2^{-\Delta\Delta CT})$.

Treg adoptive transfer to CD45.1 OT-II mice

For T reg transfer to CD45.1 OT-II mice, Tregs (CD4⁺ CD62L⁺ CD25⁺) were FACS sorted from *Atg5^{+/+}* DC or *Atg5^{-/-}* DC mice and stained with a proliferation dye. 200 000 T regs were then injected (IV) into a CD45.1 OT-II mouse. After 14 days post transfer, splenocytes were isolated and the CD45.2 proliferating Treg population was determined by flow cytometry to assess Foxp3 expression.

Time lapse Video Microscopy

BMDC generated from *Atg5^{+/+}* or *Atg5^{-/-}* mice (5×10^4) were co-cultured with CD4⁺ Foxp3^{RFP} positive or Foxp3^{RFP} negative T cells sorted from the Foxp3^{RFP}ROR γ t^{GFP} double reporter mice (1×10^5) were observed in a 8 well μ -slide (Ibidi) on a Zeiss observer.Z1 microscope with a 37°C heated stage. After 10 min, DIC images were obtained for 20min with 10 s intervals. Images were then analyzed using ImageJ software, all DC/T cell interactions above 150 s (stochastic) were taken into account for analysis. At least 100 interactions were analyzed for each condition.

For blocking experiments, cells were incubated for 10 min at 4°C with 2 μ g/ml anti-CD16/32 followed by incubation of 10 μ g/ml of anti-ICOSL (Clone HK5.3) or an isotype control for 30 min at 4°C. All DC/T cell interactions were taken into account for analysis.

Western blot

Lysates were prepared from FACS sorted Tregs (from *Atg5^{+/+}* DC and *Atg5^{-/-}* DC mice) treated with 1 μ g/ml CD3/CD28 (Bioexcel), and 1 μ g/ml LPS (Sigma) for 24h. Cells were lysed in 50 mM Tris-HCl (pH 7.5), 1% NP-40 buffer supplemented with protease inhibitors (Roche). Equal protein amounts from lysates were used after bicinchoninic acid assay quantification (Pierce). Protein samples were then denatured in Laemmli buffer, separated by SDS-polyacrylamide gel electrophoresis and transferred to PVDF membranes. Immunoblots were blocked and primary antibody for HSP70 (Sigma) was incubated in PBS supplemented with 0.05% Tween-20 (v/v) and 5% (w/v) non-fat dry milk overnight at 4°C. HRP-conjugated Goat -anti Rabbit (Biorad) was used to detect proteins by enhanced chemiluminescence.

RNA sequencing and data analysis

RNA was isolated from CD25^{High} and CD25^{Low} Treg subsets of *Atg5^{+/+}* DC or *Atg5^{-/-}* DC mice, using the RNeasy Mini kit according to manufacturer's instructions (QIAGEN). Total RNA was quantified with a Qubit (fluorimeter from Life Technologies) and RNA integrity assessed with a Bioanalyzer (Agilent Technologies). The SMARTer Ultra Low RNA kit from Clontech was used for the reverse transcription and cDNA amplification according to manufacturer's specifications, starting with 10 ng of total RNA as input. 200 pg of cDNA were used for library preparation using the Nextera XT kit from Illumina. Library molarity and quality was assessed with the Qubit and TapeStation using a DNA High sensitivity chip (Agilent Technologies). Pools of 6 libraries were loaded at 13 pM for clustering on a Single-read Illumina Flow cell. Reads of 50 bases were generated using the TruSeq SBS HS v3 chemistry on an Illumina HiSeq 2500 sequencer. FastQ reads were mapped to the ENSEMBL reference genome (GRCh38.80) using STAR version 2.4.0j (Dobin et al., 2013) with standard settings, except that any reads mapping to more than one location in the genome (ambiguous reads) were discarded ($m = 1$). A unique gene model was used to quantify reads per gene. Briefly, the model considers all annotated exons of all annotated protein coding isoforms of a gene to create a unique gene where the genomic region of all exons are considered coming from the same RNA molecule and merged together. All reads overlapping the exons of each unique gene model were reported using featureCounts version 1.4.6-p1 (Quinlan and Hall, 2010). Gene expressions were reported as raw counts and in parallel normalized in RPKM in order to filter out genes with low expression value (1 RPKM) before calling for differentially expressed genes. Library size normalizations and differential gene expression calculations were performed using the package edgeR (Robinson et al., 2010) designed for the R software. Only genes having a significant fold-change (Benjamini-Hochberg corrected p value < 0.01) were considered for the rest of the RNA sequencing analysis.

QUANTIFICATION AND STATISTICAL ANALYSIS

Statistical parameters including the exact value of n, the dispersion, the precision of measures (mean \pm sem) and the statistical significance are reported in the figures and figure legends. In all experiments, Mann Whitney unpaired non-parametric t test was

used (unless otherwise stated in the legend) using PRISM software (Version 6.01; GraphPad software). Data are presented as the mean \pm sem. The statistical significance level was set at p values, and depicted as following: *p < 0.05, **p < 0.01 and ***p < 0.00.

DATA AND CODE AVAILABILITY

Software All software are freely or commercially available and listed in the STAR METHODS

Data Resources

Data used in this manuscript are available upon request. The raw and processed RNA-seq data have been deposited to the Gene Expression Omnibus (GEO) accession number under GEO: GSE98961.